Inorganic Chemistry

Article

pubs.acs.org/IC

Complexes with Redox-Active Ligands: Synthesis, Structure, and Electrochemical and Photophysical Behavior of the Ru(II) Complex with TTF-Annulated Phenanthroline

Lawrence K. Keniley, Jr.,[†] Nathalie Dupont,[‡] Lipika Ray,[†] Jie Ding,[‡] Kirill Kovnir,[†,§] Jordan M. Hoyt,[†,∥] Andreas Hauser,*[,‡] and Michael Shatruk*[,†]

[†]Department of Chemistry and Biochemistry, Florida State University, 95 Chieftan Way, Tallahassee, Florida 32306, United States

[‡]Department of Physical Chemistry, University of Geneva, 30 quai Ernest-Ansermet, CH-1211 Geneva 4, Switzerland

Supporting Information

ABSTRACT: Ru(II) complexes with chelating ligands, 4′,5′-ethylenedithiotetrathiafulvenyl[4,5-*f*][1,10]phenanthroline (**L1**), 1,3-dithiole-2-thiono[4,5-*f*][1,10]phenanthroline (**L2**), and 1,3-dithiole-2-ono[4,5-*f*][1,10]phenanthroline (**L3**), have been prepared and their structural, electrochemical, and photophysical properties investigated. Density functional theory (DFT) calculations indicate that the highest occupied molecular orbital of $[Ru(bpy)_2(\mathbf{L1})](PF_6)_2$ (**1**) is located on the tetrathiafulvalene (TTF) subunit and appears ∼0.6 eV above the three Ru-centered d orbitals. In agreement with this finding, **1** exhibits three reversible oxidations: the two at lower potentials take place on the TTF subunit, and the one at higher potential is due to the Ru^{3+}/Ru^{2+} redox couple. Complexes $[Ru(bpy)_2(\mathbf{L2})](PF_6)_2$ (**2**) and $[Ru(bpy)_2(\mathbf{L3})](PF_6)_2$ (**3**) exhibit only the Ru^{3+}/Ru^{2+}-related oxidation. The optical absorption spectra of all complexes reveal a characteristic metal-to-ligand charge transfer (MLCT) band centered around 450 nm. In addition, in the spectrum of **1** the MLCT band is augmented by a low-energy tail that extends beyond 500 nm and is attributed to the intraligand charge transfer (ILCT) transition of **L1**, according to time-dependent DFT calculations. The substantial decrease in the luminescence quantum yield of **1** compared to those of **2** and **3** is attributed to the reductive quenching of the emissive state via electron transfer from the TTF subunit to the Ru^{3+} center, thus allowing nonradiative relaxation to the ground state through the lower-lying ILCT state. In the presence of O_2, complex **1** undergoes a photoinduced oxidative cleavage of the central C═C bond of the TTF fragment, resulting in complete transformation to **3**. This photodegradation process was studied with ^{13}C NMR and optical absorption spectroscopy.

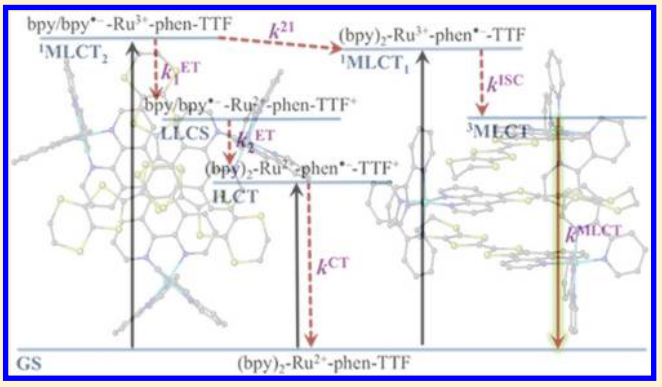

INTRODUCTION

Multifunctionality represents one of the central themes in contemporary materials science. Imparting different functions to the same material and achieving synergetic interaction between them constitute an innovative line of attack for the development of new technologies and devices.[1] Coordination chemistry provides an appealing approach to the design of multifunctional materials via simple combination of properties characteristic of a metal ion and a ligand that are bound together in the coordination compound. In this vein, complexes with ligands that contain a redox-active tetrathiafulvalene (TTF) unit have received a lot of interest in recent years because of the prospect of combining the conducting properties of the TTF substructure with magnetic, optical, or electrochemical properties of the metal ion.[2]

A number of studies have focused on the design of molecules in which a TTF-containing fragment is connected to a chelating ligand that affords robust binding to a metal ion with a geometrically predictable arrangement of the TTF subunit. In particular, TTF or its derivatives have been connected to chelating dithiolates, pyridines, phosphines, carboxylates, and *N*-heterocyclic ligands such as pyrazine, 2,2′-bipyridine, or 1,10-phenanthroline. Thiolates were the first ligands ever used to attach TTF to a metal center, for which Rivera et al. reported the preparation of a nickel(II) bis(TTF-dithiolene) complex that exhibits an unusually high room temperature conductivity of 30 S cm^{-1}.[3] Despite initial reports of a TTF-pyridine ligand in 1984,[4] it was not until 2001 that Ouahab and co-workers reported the first metal complex of TTF-pyridine in which coordination to copper(II) led to a conducting paramagnetic complex.[5] The first metal complexes to incorporate TTF-containing phosphines or carboxylates also appeared in the literature during the late 20th to the early 21st century.[6] Among the aforementioned TTF ligand

Received: March 20, 2013
Published: June 24, 2013

   dx.doi.org/10.1021/ic4006949 | *Inorg. Chem.* 2013, 52, 8040−8052

types, the *N*-heterocyclic TTF-containing ligands are of most relevance to the current work. The first successful attachment of TTF to 1,10-phenanthroline was achieved by Becher and co-workers and used to prepare precatenate complexes of Cu^{I} and Ag^{I} that act as redox responsive sensors for various metal ions.[7]

Recently, we have reported the synthesis of edt-TTF-phen (**L1**), a chelating ligand in which ethylenedithiotetrathiafulvalene (edt-TTF) is fused directly to 1,10-phenanthroline (phen), and preliminary results on the preparation and crystal structure of its Ru(II) complex.[8] Herein, we report a detailed study of the photophysical and electrochemical behavior of $[Ru(bpy)_2(\mathbf{L1})](PF_6)_2$ (**1**) and interpret its properties based on the electronic structure calculated by density functional theory (DFT) methods. We compare the behavior of **1** to that of related complexes that include only half of the TTF unit. Finally, we describe a study of an unexpected light-induced oxidative C=C bond cleavage of the TTF fragment of **1**.

EXPERIMENTAL SECTION

Spectroscopic Measurements. ^{1}H NMR spectra were measured on either a Bruker 400 or Bruker 600 spectrometer operating at 400 or 600 MHz, respectively, with chemical shifts internally referenced to the residual proton signals of the deuterated solvent $CDCl_3$ (7.26 ppm) or CD_3CN (1.94 ppm).[9] ^{13}C NMR spectra were measured on either a Mercury 300 or Bruker 600 spectrometer operating at 75.5 or 151 MHz, respectively, with chemical shifts internally referenced to the deuterated solvent signals in $CDCl_3$ (77.2 ppm) or CD_3CN (118.3 ppm).[9] Two-dimensional correlation spectroscopy (COSY) and heteronuclear single-quantum coherence ($^{1}H-^{13}C$ HSQC) experiments were carried out on a Bruker 600 spectrometer. Electrospray ionization (ESI) and electron impact (EI) mass spectra were acquired on JEOL AccuTOF JMS-T100LC and JEOL JMS600 mass spectrometers, respectively. Infrared (IR) spectra were measured in the 600−4000 cm^{-1} range as solid samples pressed on a ZnSe crystal of the universal attenuated total reflectance (ATR) sampling accessory on a Perkin-Elmer Spectrum 100 FT-IR spectrometer. Elemental analyses were carried out by Atlantic Microlab, Inc. (Norcross, GA).

Electronic absorption (UV−vis) spectra were collected in the 200−1000 nm range on a Perkin-Elmer Lambda 950 UV/vis/NIR or a Cary 50 Bio UV/vis spectrophotometer. Emission and excitation spectra were measured on a Horiba JobinYvon FluoroMax-4 spectrofluorometer. Luminescence lifetimes on the nanosecond time scale were recorded by exciting the samples at 458 nm using the third harmonic of a pulsed Nd:YAG laser (Quantel Brilliant, 7 ns pulse width) to pump an optical parametric oscillator (Opotek Magic Prism). The system used for detection consisted of a single monochromator (Spex 270M), a photomultiplier (Hamamatsu R928), and a digital oscilloscope (Tektronix TDS 540B) with a time resolution of 15 ns. The reported values for the luminescence quantum yields of complexes **1**−**3** were calculated using $[Ru(bpy)_3](PF_6)_2$ as a standard with a quantum yield of 6.2% in CH_3CN at room temperature.

Electrochemistry. Cyclic voltammetry (CV) was performed on a CH Instruments 600D electrochemical analyzer at a sweep rate of 0.100 V s^{-1} with a 0.100 M $(Bu_4N)PF_6$ electrolyte solution, a Pt disk working electrode, a Pt wire counter electrode, and a Ag^{+}(0.01 M $AgNO_3$)/Ag nonaqueous reference electrode. All the potentials were referenced to the standard Fc^{+}/Fc couple (Fc = ferrocene). Fc was added as an internal standard upon completion of each CV experiment.

Synthesis. All reactions were performed in an inert N_2 atmosphere using standard Schlenk techniques, unless noted otherwise. Commercially available 1,10-phenanthroline (99%), fuming sulfuric acid (20% SO_3), bromine (99.5%), carbon disulfide (anhydrous, 99.9%), potassium (poly)sulfide (>42% K_2S basis), mercury(II) acetate (99%, Aldrich), glacial acetic acid (EMD), sodium bicarbonate (99%, Mallinckrodt), and 4,5-ethylenedithio-1,3-dithiol-2-thione (TCI) were used as received. Triethylphosphite (98%, Aldrich) was distilled under nitrogen prior to use. 4,5-Ethylenedithio-1,3-dithiol-2-one was prepared according to the published procedure.[10] Additional purification of anhydrous commercial solvents used in anaerobic reactions was achieved by passing them through a double-stage drying/purification system (Glass Contour Inc.). Otherwise, ACS grade solvents were used.

5,6-Dibromo-1,10-phenanthroline (Br_2phen). A 100 mL heavy-wall pressure vessel was cooled in an ice bath and charged with 5.45 g (30.2 mmol) of 1,10-phenanthroline and 44 mL of fuming sulfuric acid; 1.55 mL of bromine (30.2 mmol) was added with a pipet, and the vessel was closed tightly with a Teflon bushing equipped with a chemically resistant O-ring. The vessel was immersed in an oil bath preheated to 120 °C. After being allowed to react for 12 h at constant temperature, the mixture was cooled to room temperature. The deep red solution obtained was poured carefully into 1.5 L of chilled water with vigorous stirring, and the pH was adjusted to 3 with sodium bicarbonate, resulting in precipitation of a solid product. (It is essential that the pH remains below 3.0 to avoid contamination of the desired product with 1,10-phenanthroline-5,6-dione byproduct.) After filtration, the filter cake was extracted with CH_2Cl_2 (3 × 130 mL). The solution was dried over $MgSO_4$ and evaporated to dryness. The product can be recrystallized from ethanol to afford white needles, but the fluffy white powder (crude product) proved to be of sufficient purity to be used in the subsequent reactions. Yield: 62% (6.33 g). Anal. Calcd (found) for $C_{12}H_6N_2Br_2$, wt %: C, 42.64 (43.04); H, 1.79 (1.89); Br, 47.28 (46.91); N, 8.29 (8.13). ^{1}H NMR ($CDCl_3$, 600 MHz) δ: 9.20 (dd, 2H, J = 1.5, 5.7 Hz), 8.76 (dd, 2H, J = 1.6, 10.0 Hz), 7.72 (dd, 2H, J = 4.3, 12.6 Hz). ESI-MS, m/z (relative intensity): 339 ($[M + 1]^{+}$, 100), 260 ($[M - Br + 2H]^{+}$, 4).

*1,3-Dithiole-2-thiono[4,5-f][1,10]phenanthroline (**L2**).* The compound was prepared according to the literature method with a slight modification of the workup procedure.[11] The yellow solid obtained from successive extractions with $CHCl_3$ contained the desired product **L2** contaminated with the starting material Br_2phen. The latter was removed by washing the mixture with hot ethanol. Yield: 96%. Anal. Calcd (found) for $C_{13}H_8N_2OS_3$ (**L2**·H_2O), wt %: C, 51.29 (51.29); H, 2.65 (2.53); N, 9.20 (9.16); S, 31.60 (31.35). ^{1}H NMR ($CDCl_3$, 600 MHz) δ: 9.26 (dd, 2H, J = 1.6, 5.9 Hz), 8.08 (dd, 2H, J = 1.6, 9.8 Hz), 7.74 (dd, 2H, J = 4.3, 12.5 Hz). EI-MS, m/z (relative intensity): 286 ($[M]^{+}$, 100), 242 ($[M - CS]^{+}$, 25), 210 ($[M - CS_2]^{+}$, 18). IR (ZnSe ATR), ν, cm^{-1}: 642 (m), 736 (vs), 804 (s), 918 (m), 1063 (s), 1093 (C=S, vs), 1414 (s), 1477 (w), 1495 (m), 1569 (m), 1682 (s), 2954 (w).

*1,3-Dithiole-2-ono[4,5-f][1,10]phenanthroline (**L3**).* To a clear yellow solution of 123 mg (0.429 mmol) of **L2** in 150 mL of $CHCl_3$ were added sequentially 200 mL of glacial acetic acid and 342 mg (1.07 mmol) of $Hg(OAc)_2$. The solution turned to a white cloudy suspension within 5 min. The suspension was stirred for 3 h at room temperature. The white precipitate was removed by filtration. The clear and colorless organic phase was washed with an equal volume of H_2O, three times with an equal volume of a saturated aqueous $NaHCO_3$ solution, and finally with an equal volume of H_2O. The resulting $CHCl_3$ solution was dried over $MgSO_4$ and evaporated to dryness to afford **L3** as a white solid. Yield: 98% (113 mg). ^{1}H NMR ($CDCl_3$, 400 MHz) δ: 9.24 (dd, 2H, J = 1.6, 6.0 Hz), 8.11 (dd, 2H, J = 1.6, 9.8 Hz), 7.73 (dd, 2H, J = 4.3, 12.6 Hz). IR (ZnSe ATR), ν, cm^{-1}: 732 (vs), 790 (vs), 915 (m), 1016 (m), 1259 (m), 1414 (s), 1472 (w), 1490 (m), 1640 (vs), 1701 (C=O, m), 2919 (w).

*4′,5′-Ethylenedithiotetrathiafulvenyl[4,5-f][1,10]phenanthroline (**L1**).* A mixture of 222 mg (0.775 mmol) of **L2**, 484 mg (2.33 mmol) of 4,5-ethylenedithio-1,3-dithiol-2-one, and 10 mL of $P(OEt)_3$ was placed in a Schlenk tube and heated at reflux under N_2 for 12 h. After cooling to room temperature, the obtained red precipitate was filtered off, washed with cold methanol (3 × 20 mL), and dried under vacuum. The product was loaded onto a 1 in. bed of silica gel and washed with CH_2Cl_2 to remove byproducts. Then the eluent was gradually changed to CH_2Cl_2/MeOH (2:1 v/v), and the collected fraction was filtered through Celite and evaporated to dryness to afford pure **L1** as an orange solid. Yield: 54% (187 mg). Recrystallization from $CHCl_3$/hexanes resulted in orange crystals of **L1**·$CHCl_3$. Anal. Calcd (found) for $C_{19}H_{11}N_2S_6Cl_3$ (**L1**·$CHCl_3$), wt %: C, 40.32 (40.37); H, 1.96 (1.89); N, 4.95 (5.15); S, 33.99 (33.64). ^{1}H NMR ($CDCl_3$, 600 MHz) δ: 9.17 (dd, 2H, J = 1.6, 5.9 Hz), 8.01 (dd, 2H, J = 1.6, 9.8 Hz), 7.68 (dd, 2H, J = 4.3, 12.5 Hz), 3.34 (s, 4H, CH_2). ^{13}C NMR ($CDCl_3$, 75.5 MHz) δ: 30.5, 80.6, 114.3, 123.9,

dx.doi.org/10.1021/ic4006949 | Inorg. Chem. 2013, 52, 8040−8052

Table 1. Data Collection and Structure Refinement Parameters for L1·$CHCl_3$, L2, 1·3.6CH_3CN, and 3·0.8CH_3CN

	$C_{19}H_{11}N_2S_6Cl_3$ (**L1**·$CHCl_3$)	$C_{13}H_6N_2S_3$ (**L2**)	$C_{45.2}H_{36.8}N_{9.6}Ru_1S_6P_2F_{12}$ (**1**·3.6CH_3CN)	$C_{34.6}H_{24.4}N_{6.8}O_1Ru_1S_2P_2F_{12}$ (**3**·0.8CH_3CN)
CCDC number	718515	718514	751678	751912
space group	$P2_12_12_1$	$P2_1/c$	$P2_1/c$	$P\bar{1}$
unit cell parameters (Å and deg)	a = 7.127(1)	a = 3.851(1)	a = 22.57(2)	a = 8.928(3)
	b = 17.269(3)	b = 10.297(3)	b = 22.54(2)	b = 12.162(4)
	c = 18.462(3)	c = 28.547(9)	c = 32.53(3)	c = 17.426(5)
		β = 91.511(4)	β = 92.07(1)	α = 89.738(4)
				β = 86.754(4)
				γ = 83.664(4)
V (Å^3)	2272.2(7)	1131.7(6)	16539(26)	1878(1)
Z	4	4	12	2
ρ_{calc} (g cm^{-3})	1.655	1.681	1.563	1.778
T (K)	173	173	173	173
λ (Mo Kα, Å)	0.71093	0.71093	0.71093	0.71093
μ (mm^{-1})	0.967	0.632	0.653	0.716
$2\theta_{max}$ (deg)	52.8	52.8	52.0	52.0
reflections collected	21876	7011	62897	19226
R_{int}	0.138	0.063	0.082	0.046
unique reflns	4652	2295	31363	7312
parameters/restraints	322/0	163/0	1938/6	528/0
R_1, wR_2 [$F_o > 4\sigma F_o$]	0.051, 0.075	0.042, 0.077	0.073, 0.178	0.054, 0.138
goodness of fit	0.952	0.975	0.962	1.019
diff. peak and hole (e/Å^3)	0.35 and −0.39	0.35 and −0.34	1.26 and −0.80	1.20 and −0.54

124.2, 131.0, 133.3, 145.3, 150.2. ESI-MS, m/z (relative intensity): 916 ([2M + Na]$^+$, 14), 470 ([M + Na]$^+$, 30), 447 ([M]$^+$, 100), 419 ([M − C_2H_4]$^+$, 11). UV−vis (CH_2Cl_2), λ_{max}, nm (log ε): 232 (4.48), 277 (4.37), 310 (4.24), 336 (4.08), 403 (3.51). IR (ZnSe ATR), ν, cm^{-1}: 660 (w), 737 (vs), 769 (m), 790 (m), 917 (s), 1146 (w), 1400 (w), 1418 (s), 1479 (w), 1576 (m), 2934 (w).

*[Ru(bpy)$_2$(**L1**)](PF$_6$)$_2$ (**1**).* A suspension of **L1** (50 mg, 0.112 mmol) in anhydrous ethanol (10 mL) was added to a suspension of [Ru(bpy)$_2$Cl$_2$]·2H_2O (53 mg, 0.102 mmol) in anhydrous ethanol (15 mL). The mixture was refluxed in the dark under N_2 for 12 h, after which the reaction mixture was cooled to room temperature and filtered. A solution of NH_4PF_6 (58 mg, 0.356 mmol) in anhydrous ethanol (25 mL) was added dropwise to the filtrate. The solution was left undisturbed overnight at −23 °C, resulting in precipitation of a brown product. Yield: 76% (89 mg). X-ray quality single crystals were obtained by vapor diffusion of diethyl ether into an acetonitrile solution of the complex in the dark. Anal. Calcd (found) for $RuC_{38}H_{28}N_6O_1S_6P_2F_{12}$ (**1**·1H_2O), %: C, 39.07 (39.19); H, 2.42 (2.42); N, 7.19 (7.40); S, 16.47 (16.30). ^{1}H NMR (CD_3CN, 600 MHz) δ: 8.55 (d, 2H, J = 8.2 Hz), 8.52 (d, 2H, J = 8.1 Hz), 8.11 (td, 2H, J = 1.4, 17.4 Hz), 8.05 (m, 4H), 7.98 (dd, 2H, J = 0.9, 9.2 Hz), 7.84 (dd, 2H, J = 0.7, 6.2 Hz), 7.66 (m, 4H), 7.47 (m, 2H), 7.34 (m, 2H), 3.32 (d, 4H, J = 3.0 Hz). ^{13}C NMR (CD_3CN, 151 MHz) δ: 158.7, 158.4, 153.8, 153.6, 153.4, 148.5, 139.5, 139.5, 134.7, 134.5, 129.1, 129.1, 128.3, 127.0, 125.8, 125.8, 115.1, 113.3, 66.7, 16.1. ESI-MS (CH_3OH), m/z (M = [Ru(bpy)$_2$(**L1**)]$^{2+}$, relative intensity): 1005 ([M + PF_6]$^+$, 100), 481 ([M − **L1** + Cl + CH_3OH]$^+$, 52), 449 ([M − **L1** + Cl]$^+$, 30), 430 ([M]$^{2+}$, 24), 416 ([M − C_2H_4]$^{2+}$, 41). UV−vis (CH_3CN), λ_{max}, nm (log ε): 240 (4.73), 253 (4.66), 285 (4.87), 343 (4.06), 450 (4.18). Emission (CH_3CN, λ_{exc} = 450 nm), λ_{max}, nm (quantum yield, Φ_F): 636 (0.012).

The complexes [Ru(bpy)$_2$(**L2**)](PF$_6$)$_2$ (**2**) and [Ru(bpy)$_2$(**L3**)](PF$_6$)$_2$ (**3**) were prepared in a similar manner as described above for complex **1**.

*[Ru(bpy)$_2$(**L2**)](PF$_6$)$_2$ (**2**).* Yield: 93%. Anal. Calcd (found) for $RuC_{33}H_{23}N_6O_{0.5}S_3P_2F_{12}$ (**2**·0.5H_2O), %: C, 39.68 (39.75); H, 2.32 (2.33); N, 8.41 (8.73); S, 9.63 (9.44); F, 22.64 (22.75). ^{1}H NMR (CD_3CN, 600 MHz) δ: 8.53 (d, 2H, J = 8.0 Hz), 8.50 (d, 2H, J = 8.0 Hz), 8.39 (dd, 2H, J = 1.1, 9.5 Hz), 8.15 (dd, 2H, J = 1.1, 6.4 Hz), 8.10 (td, 2H, J = 1.4, 17.3 Hz), 8.02 (td, 2H, J = 1.4, 17.3 Hz), 7.81 (d, 2H, J = 5.6 Hz), 7.78 (dd, 2H, J = 5.3, 13.7 Hz), 7.56 (d, 2H, J = 5.0 Hz), 7.45 (m, 2H), 7.25 (m, 2H). UV−vis (CH_3CN), λ_{max}, nm (log ε): 255 (4.62), 287 (4.85), 372 (4.36), 385 (4.30), 445 (4.21). Emission (CH_3CN, λ_{exc} = 450 nm), λ_{max}, nm (quantum yield, Φ_F): 632 (0.066).

*[Ru(bpy)$_2$(**L3**)](PF$_6$)$_2$ (**3**).* Yield: 78%. Anal. Calcd (found) for $RuC_{33}H_{27}N_6O_{3.5}S_2P_2F_{12}$ (**3**·2.5H_2O), %: C, 38.91 (38.87); H, 2.67 (2.56); N, 8.25 (8.25); S, 6.30 (6.16). ^{1}H NMR (CD_3CN, 600 MHz) δ: 8.53 (d, 2H, J = 8.1 Hz), 8.49 (d, 2H, J = 8.2 Hz), 8.40 (dd, 2H, J = 1.1, 9.5 Hz), 8.13 (dd, 2H, J = 1.1, 6.4 Hz), 8.10 (td, 2H, J = 1.4, 17.3 Hz), 8.01 (td, 2H, J = 1.5, 17.3 Hz), 7.81 (d, 2H, J = 4.9 Hz), 7.77 (dd, 2H, J = 5.3, 13.7 Hz), 7.55 (d, 2H, J = 5.0 Hz), 7.44 (m, 2H), 7.24 (m, 2H). ^{13}C NMR (CD_3CN, 151 MHz) δ: 187.9, 158.2, 158.0, 154.0, 153.1, 153.0, 147.8, 139.1, 139.0, 134.9, 130.5, 128.7, 128.5, 128.0, 127.4, 125.4, 125.3. UV−vis (CH_3CN), λ_{max}, nm (log ε): 256 (4.61), 285 (4.95), 340 (3.94), 449 (4.16). Emission (CH_3CN, λ_{exc} = 450 nm), λ_{max}, nm (quantum yield, Φ_F): 628 (0.097).

X-ray Crystallography. In a typical experiment, a selected single crystal was suspended in Paratone-N oil (Hampton Research) and mounted on a cryoloop, which was placed in an N_2 cold stream and cooled at 5 K/min to 173 K. The data sets were recorded as ω-scans at 0.3° step width and integrated with the Bruker SAINT software package.[12] In all the experiments, a multiscan adsorption correction was applied based on fitting a function to the empirical transmission surface as sampled by multiple equivalent measurements (SADABS).[13] Determination of the space group, solution, and refinement of the crystal structures was carried out using the SHELX suite of programs.[14] The final refinement was performed with anisotropic atomic displacement parameters for all but hydrogen atoms. The H atoms were placed in calculated positions. A summary of pertinent information relating to unit cell parameters, data collection, and refinements is provided in Table 1.

Theoretical Calculations. DFT calculations were performed with the Gaussian 03 package[15] using the B3LYP hybrid functional[16] and the LanL2DZ basis set.[17] Starting geometries for complexes **1**−**3** were taken from the refined crystal structure parameters. All geometries were optimized in the ground state without symmetry restraints. Single-point time-dependent DFT (TD-DFT) calculations were carried out on the optimized geometries using the conducting polarized continuum medium (CPCM, CH_3CN) solvation model to include solvent polarization effects. The UV−vis spectra were calculated with the SWizard program, revision 4.7,[18] using the pseudo-Voigt model. The half-bandwidths, $\Delta_{1/2}$, were set equal to 3000 cm^{-1}. Molecular fragment

dx.doi.org/10.1021/ic4006949 | Inorg. Chem. 2013, 52, 8040−8052

Scheme 1. Synthesis of L1−L3 and Their Ru(II) Complexes 1−3[a]

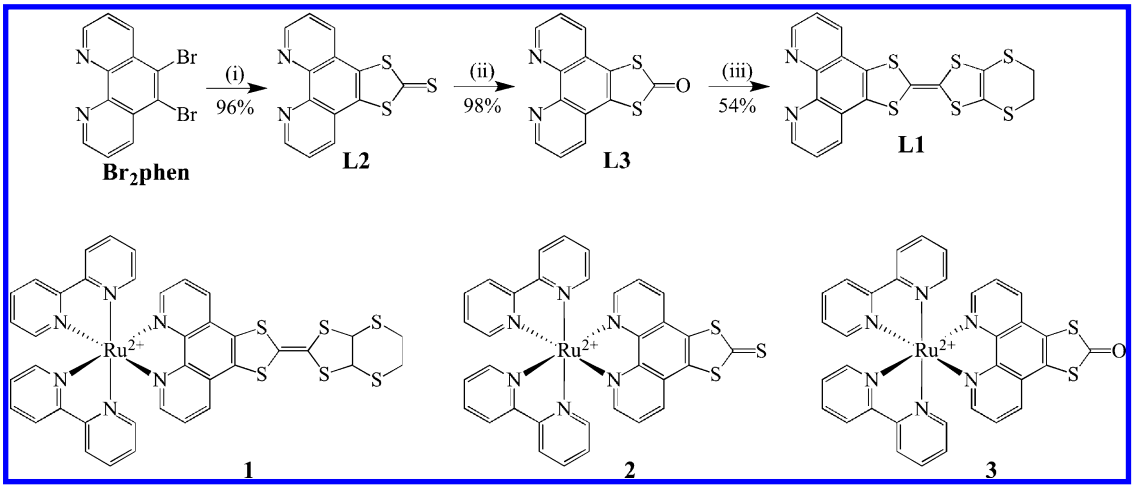

[a](i) K_2S, CS_2, DMF, 60 °C, 36 h; (ii) $Hg(O_2CCH_3)_2$, CH_3CO_2H, $CHCl_3$, 3 h; (iii) 4,5-ethylenedithio-1,3-dithiole-2-one, $P(OEt)_3$, reflux, 12 h.

contributions to frontier orbitals were calculated using the AOMix program.[18b,19]

RESULTS AND DISCUSSION

Synthesis. The synthetic pathway toward ligands **L1**−**L3** is outlined in Scheme 1. Ligand **L2** can be prepared in several ways. The approaches, reported by Almeida and co-workers,[20] Hudhomme and co-workers,[21] and our group,[8] proceed via substitution of benzylthiolates for the bromo substituents in Br_2phen. The benzyl groups are then cleaved with *t*-BuOK or $AlCl_3$, and the generated dithiolate can be converted to the 1,3-dithiole-2-thione ring with thiophosgene or CS_2 under basic conditions. Despite relatively good yields (~32% based on Br_2phen), these methods require multistep synthesis and the use of hazardous benzylmercaptan. Recently, Qin et al. demonstrated that **L2** can be prepared in high yield by simply treating Br_2phen with K_2CS_3 in DMF.[11] This route provides a simple and inexpensive one-pot reaction for the preparation of **L2**. Nevertheless, our attempts to repeat the published procedure led consistently to a mixture of **L2** and unreacted Br_2phen, but the latter can be easily removed because of its solubility in hot ethanol. The conversion from **L2** to **L3** is achieved by a standard synthetic protocol that includes treating the solution of **L2** in $CHCl_3$ and glacial acetic acid with $Hg(OAc)_2$.[22]

The ligands **L2** and **L3** provide an entry into the synthetic chemistry of TTF-annulated phenanthrolines, as demonstrated by our preparation of the asymmetric ligand **L1** via a triethylphosphite-mediated cross-coupling reaction between **L2** and 4,5-ethylenedithio-1,3-dithiole-2-one (Scheme 1).[23] The same result can be obtained by reacting **L3** and 4,5-ethylenedithio-1,3-dithiole-2-thione in triethylphosphite. A separation of **L1** from the symmetric byproduct, bis(ethylenedithio)-tetrathiafulvalene (BEDT-TTF), formed by self-coupling of 4,5-ethylenedithio-1,3-dithiole-2-one, is achieved by using a short column (2.5 cm) and washing out the BEDT-TTF impurity with CH_2Cl_2, after which the eluent is switched to CH_2Cl_2/CH_3OH (2:1 v/v) to wash out the pure **L1** fraction.

Because of the never-diminishing interest in ruthenium(II) complexes that incorporate *N*-heterocyclic polypyridyl ligands, we were incited to investigate the electrochemical and photophysical properties of such complexes prepared with ligands **L2** and **L3** and especially with the redox-active ligand **L1**. Reactions between these ligands and $[Ru(bpy)_2Cl_2]$ in refluxing ethanol result in the formation of the desired complexes that can be isolated as hexafluorophosphate salts, $[Ru(bpy)_2(\mathbf{L}_i)](PF_6)_2$ (i = 1, 2, or 3) upon addition of an excess of NH_4PF_6. The crystals of these complexes are obtained by slow diffusion of diethyl ether into an acetonitrile solution of the complex.

NMR Spectroscopy. All ligands and complexes were unambiguously characterized by NMR spectroscopy. The ^{1}H NMR spectra of all ligands exhibit three distinct series of peaks in the aromatic region that can be explicitly assigned to the protons on the phenanthroline moiety (Figure 1). The ^{1}H NMR spectrum of **L1** shows that the H_a proton of the phen moiety resonates at lowest field (δ = 9.17 ppm), followed by the H_b proton (δ = 8.01 ppm) and the more shielded H_c proton (δ = 7.68 ppm).

In addition to 1D NMR experiments, complexes **1**−**3** were also examined by 2D ^{1}H COSY and ^{1}H−^{13}C HSQC methods that allowed unequivocal assignment of signals in the more complicated aromatic region (Supporting Information, Figure S1). This region contains signals that can be assigned to the bipyridine and phenanthroline moieties. Upon coordination of phenanthroline-based ligands to the Ru(II) center, the most dramatic changes are observed for the α-protons, whose signals are shifted upfield by ~1.2 ppm. This shift can be explained by shielding arising from the proximity of these protons to the π-system of bipyridine ligands (Supporting Information, Figure S2), which is a commonly observed effect in such complexes with chelating polypyridyl ligands. The ^{1}H NMR spectrum shows that the two bipyridine ligands are magnetically equivalent and thus produce eight signals that can be identified with four protons from each pyridyl moiety. The bipyridine protons were assigned in accordance with previously reported NMR assignments for ruthenium polypyridyl complexes.[24]

Crystal Structure. The ligand **L1** crystallizes in the chiral orthorhombic space group $P2_12_12_1$. The chirality stems not from the molecular structure but from the crystal packing. A careful examination of the crystal structure did not reveal any additional symmetry. The crystal structure refinement revealed that the compound crystallizes as a racemic twin. The dark orange crystals exhibit rod-shaped morphology and contain an interstitial solvent molecule, resulting in the formula **L1**·$CHCl_3$. In the crystal structure, the molecule of **L1** is almost planar (Figure 2a). The rms deviation from a least-squares plane through all atoms is 0.035(6) Å, excluding the peripheral ethylenedithio (edt)

dx.doi.org/10.1021/ic4006949 | Inorg. Chem. 2013, 52, 8040−8052

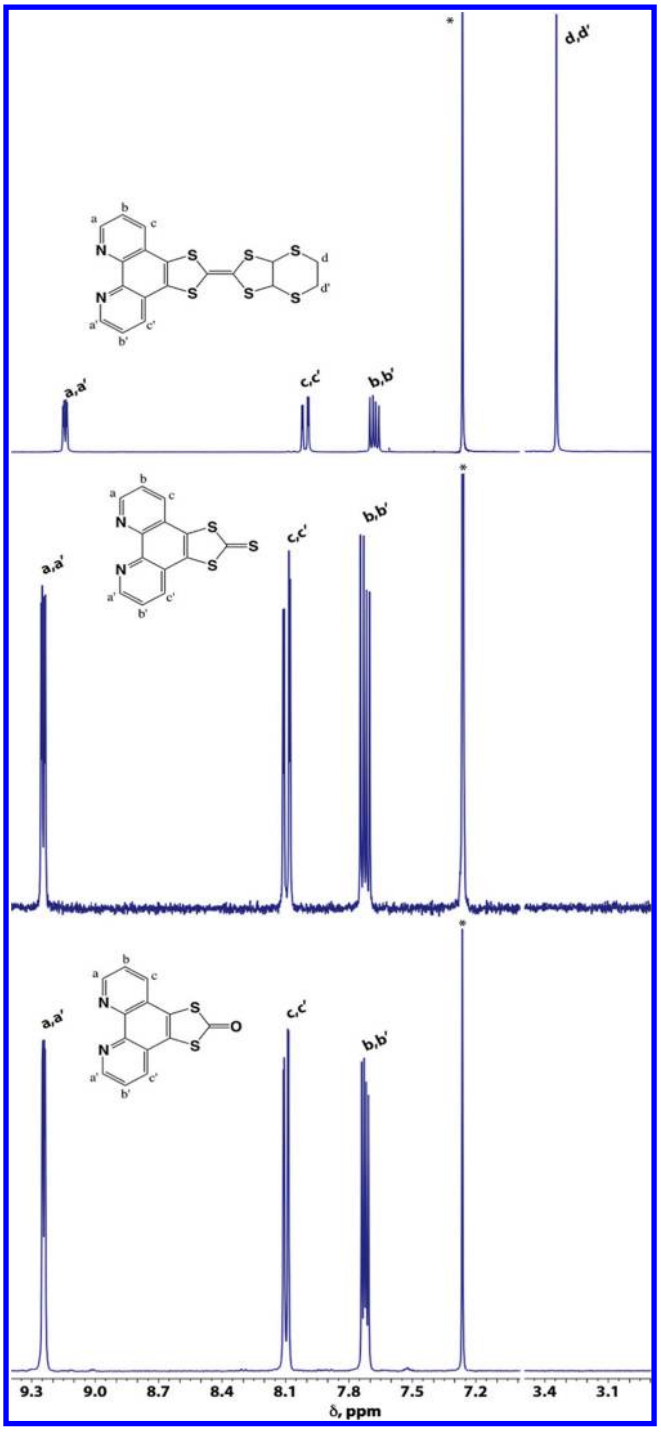

Figure 1. Selected aromatic and aliphatic regions of the ^{1}H NMR spectra of **L1**−**L3** (top to bottom, respectively; $CDCl_3$, room temperature). The residual solvent signal is marked with an asterisk.

subunit, the carbon atoms of which are disordered over two positions ∼0.4 Å above and below the molecular plane. The molecules are stacked in columns parallel to the *a* axis in a head-to-tail fashion (Supporting Information, Figure S3) and exhibit face-to-face $\pi-\pi$ contacts with an interplanar separation of 3.56 Å. Large channels are present along the *a* axis, which are filled with disordered $CHCl_3$ molecules.

The mononuclear complex $[Ru(bpy)_2(\mathbf{L1})](PF_6)_2$ (**1**) crystallizes as a dark red acetonitrile solvate, **1**·3.6CH_3CN (Figure 2b), in the centrosymmetric monoclinic space group $P2_1/c$. Similar to the structure of **L1**, the ligand remains nearly planar in the structure of **1**·3.6CH_3CN, with a 0.12(5) Å rms deviation from a least-squares plane fit through all atoms but the carbon atoms of the edt fragment. The crystal packing features a unique stacking motif of TTF moieties propagating along the *b* axis (Figure 2c,d). An asymmetric unit includes three $[Ru(bpy)_2(\mathbf{L1})]^{2+}$ dications of the same chirality. An inversion operation generates three dications of the opposite chirality, resulting in a stacking of alternating "triplets" of Δ- and Λ-isomers, with six dicationic species in a repeat unit of the stack. Thus, the overall structure is indeed centrosymmetric. The plane-to-plane separation between TTF units varies from 3.44 to 3.78 Å.

The crystals of **1**·3.6CH_3CN quickly lose crystallinity when removed from mother liquor, which can be explained by the loss of interstitial solvent. The crystals remain indefinitely stable when kept under mother liquor in the dark, but when exposed to light in the presence of air, these dark red crystals gradually convert to bright orange crystals of **3**·0.8CH_3CN. This conversion is described in detail in Photodegradation of the TTF-Containing Complex 1.

Electrochemistry. The electrochemical properties of ligand **L1** and complexes **1**−**3** were investigated in a CH_3CN/CH_2Cl_2 (3:2 v/v) solution (Table 2). Ligand **L1** exhibits two reversible one-electron redox processes that are associated with the successive oxidations of the TTF subunit to the radical cation $TTF^{+\bullet}$ and the dication TTF^{2+} (Figure 3). The half-wave potentials of **L1** (0.17 and 0.52 V vs Fc^+/Fc) are positively shifted relative to those observed for unsubstituted TTF (−0.10 and 0.27 V),[25] as expected from the π-accepting nature of the phenanthroline moiety.

The corresponding Ru(II) complex **1** exhibits three reversible oxidation processes (Figure 3), in contrast to complexes **2** and **3**, which exhibit only one reversible oxidation (Table 2). A comparison of the redox behavior of **1** to that of **2**, **3**, and **L1** indicates that the first two one-electron oxidations in **1** (at 0.26 and 0.58 V) are TTF-based. They are shifted to slightly more positive potentials relative to those observed for **L1** because of the electrostatic inductive effect of the Ru(II) ion bound to **L1**. The third oxidation for complex **1** at 1.04 V corresponds to the $Ru^{3+/2+}$ redox couple, as does the only oxidation observed for either **2** or **3**, at 0.97 and 0.96 V, respectively. This couple is also the only oxidation observed for the reference compound $[Ru(bpy)_2(phen)](PF_6)_2$ at 0.89 V (Table 2).[26] All three oxidations in **1** are similar to those reported earlier for $[Ru(bpy)_2(TTF\text{-}dppz)](PF_6)_2$ (0.29, 0.61, and 0.99 V).[27] Two reversible one-electron reduction waves were observed for **1** in the cathodic region (at −1.54 and −1.92 V). They are also comparable to the reversible reductions observed for the reference compounds, $[Ru(bpy)_2(phen)](PF_6)_2$ (−1.71 and −1.91 V) and $[Ru(bpy)_2(TTF\text{-}dppz)](PF_6)_2$ (−1.35 and −1.79 V), and attributed to the reduction of the phenanthroline and bipyridine moieties, respectively.

Electronic Structure. DFT and TD-DFT calculations have been shown to be indispensible for the analysis of photophysical behavior of Ru(II) polypyridyl complexes.[28] Therefore, we carried out such calculations to elucidate the electronic structure of complexes **1**−**3** and aid in the interpretation of their photophysical properties. The energy diagram of selected frontier molecular orbitals (MOs) appears in Figure 4, while the corresponding orbital energies for each complex are listed in Table 3.

dx.doi.org/10.1021/ic4006949 | *Inorg. Chem.* 2013, 52, 8040−8052

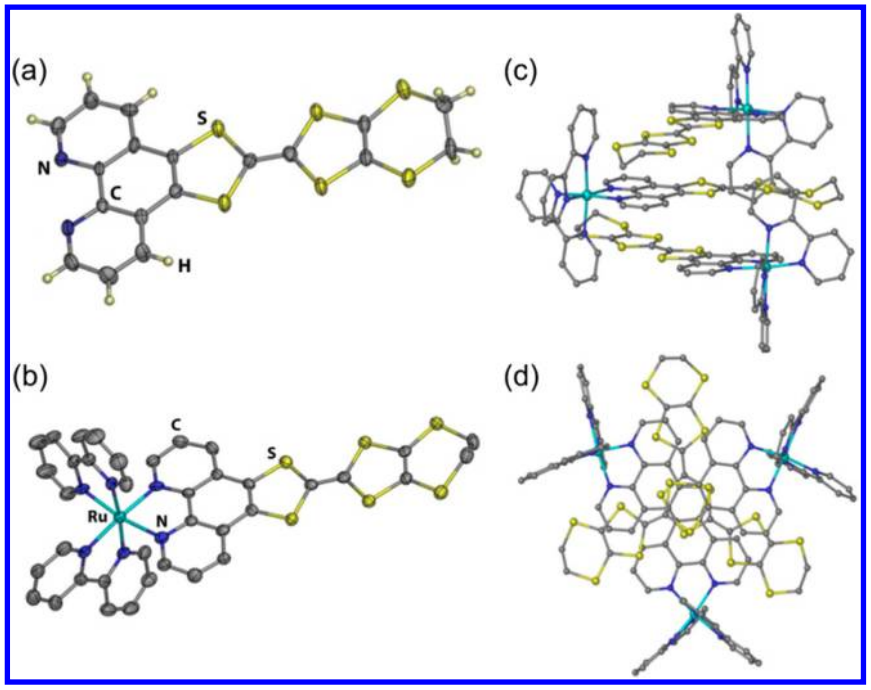

Figure 2. (a, b) Molecular structures of ligand **L1** and its Ru(II) complex, $[Ru(bpy)_2(\mathbf{L1})]^{2+}$. Thermal ellipsoids are at the 50% probability level. (c, d) Side and top views of the packing of $[Ru(bpy)_2(\mathbf{L1})]^{2+}$ cations in the crystal structure of $\mathbf{1}\cdot 3.6CH_3CN$. In b–d, the H atoms have been omitted for clarity. Color scheme: Ru, light blue; S, yellow; N, blue; C, gray; H, off-white.

Table 2. Redox Potentials (V vs Fc^+/Fc) of Ligand L1 and Complexes 1–3 in CH_3CN/CH_2Cl_2 (3:2 v/v) and of Reference Compounds TTF in CH_2Cl_2,[25] $[Ru(bpy)_2(phen)](PF_6)_2$ in CH_3CN,[26] and $[Ru(bpy)_2(TTF\text{-}dppz)](PF_6)_2$ in CH_2Cl_2/CH_3CN (5:1)[27]

compound	oxidation			reduction	
	$E_{1/2}^{(1)}$	$E_{1/2}^{(2)}$	$E_{1/2}^{(3)}$	$E_{1/2}^{(1)}$	$E_{1/2}^{(2)}$
L1	0.17	0.52			
1	0.26	0.58	1.04	−1.54	−1.92
2			0.97	−1.80	−2.03
3			0.96	−1.84	−2.04
TTF	−0.10	0.37			
$[Ru(bpy)_2(phen)](PF_6)_2$			0.89	−1.71	−1.91
$[Ru(bpy)_2(TTF\text{-}dppz)](PF_6)_2$	0.29	0.61	0.99	−1.35	−1.79

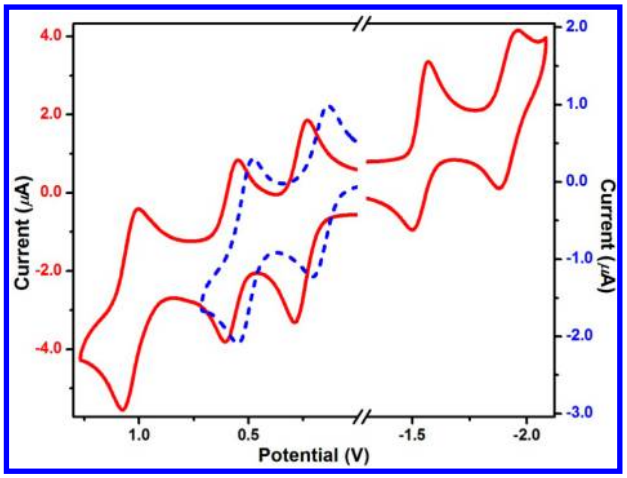

Figure 3. Cyclic voltammograms of **L1** and **1** (dashed blue and solid red lines, respectively) recorded in a 0.100 M solution of $(Bu_4N)PF_6$ in CH_3CN/CH_2Cl_2 (3:2 v/v) at 0.100 V/s. Potentials are given vs Fc/Fc^+.

The most obvious difference between the three complexes appears in the nature of the highest occupied MOs (HOMOs). Complexes **2** and **3** are characterized by the presence of metal-based HOMO, HOMO−1, and HOMO−2, corresponding to the d orbitals of the Ru ion, as typical of many Ru polypyridyl complexes. These three orbitals are preserved in complex **1**, but about 0.6 eV above them lies the new π-type HOMO centered entirely on the TTF fragment. This finding is in agreement with the observation of two TTF-centered oxidations that precede the $Ru^{3+/2+}$ redox couple in **1**. The purely TTF-based HOMO and essentially unchanged nature of the metal-centered orbitals in **1** as compared to that of **2** and **3** (Table 3) indicate that the electronic coupling between the Ru^{II} ion and the TTF fragment is negligible.

In all three complexes, below the three metal-based orbitals appear ligand-centered π orbitals. In **2** and **3**, the HOMO−3 is localized on the dithiocarbonate-phenanthroline (DTC-phen) and trithiocarbonate-phenanthroline (TTC-phen) fragments, respectively, while in **1** the HOMO−4 is centered on the TTF-phen.

The four lowest unoccupied MOs (LUMOs) are similar in all three complexes, corresponding to π^* orbitals of polypyridyl ligands and spanning a range of only ~0.2 eV. The LUMO and LUMO+1 are centered almost entirely on the phenanthroline fragment. The LUMO+2, LUMO+3, and LUMO+4 are largely bipyridine-based, with the exception of LUMO+3 in **2**, which is centered on **L2**. It appears that the change from the C═C and C═O bonds in **1** and **3**, respectively, to the C═S bond in **2** results in the lower energy of the **L2**-centered π^* orbital, which has an important ramification on the appearance of the optical absorption spectrum of **2**, as discussed below.

Optical Spectra. The optical absorption spectra of **1**–**3** are similar, revealing three major bands centered around 35000,

dx.doi.org/10.1021/ic4006949 | Inorg. Chem. 2013, 52, 8040–8052

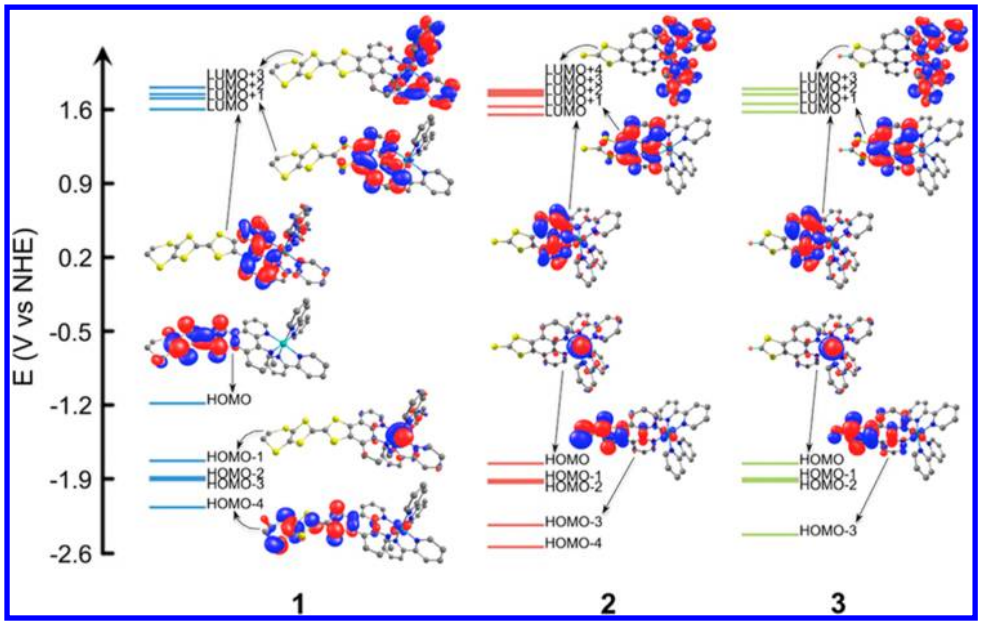

Figure 4. Frontier molecular orbitals of **1**−**3**. H atoms have been omitted for clarity. All energies have been converted to the normal hydrogen electrode (NHE) scale assuming that the NHE potential is −4.5 V vs vacuum level.[29]

Table 3. Energies (in eV)[a] and Composition (in %) of Frontier Molecular Orbitals of 1−3[b]

	1				2				3			
MOs	energy	Ru	L1	bpy	energy	Ru	L2	bpy	energy	Ru	L3	bpy
L+4	2.52	0.90	9.45	89.65	1.79	5.62	1.95	92.43	2.50	0.71	22.79	76.50
L+3	1.81	5.39	4.43	90.18	1.76	0.16	96.46	3.38	1.80	5.57	2.53	91.89
L+2	1.76	4.79	14.89	80.33	1.73	3.95	11.71	84.35	1.74	4.43	10.76	84.81
L+1	1.72	1.39	94.71	3.90	1.63	1.12	97.24	1.65	1.66	1.20	96.62	2.18
L	1.61	2.06	80.08	17.86	1.56	2.83	86.43	10.74	1.58	2.52	84.09	13.39
H	−1.16	0.05	99.93	0.02	−1.76	82.58	5.37	12.06	−1.75	82.60	5.42	11.99
H−1	−1.73	82.68	5.38	11.94	−1.91	70.14	18.98	10.88	−1.90	72.32	16.36	11.33
H−2	−1.87	69.43	19.70	10.87	−1.93	76.30	3.74	19.96	−1.92	76.30	3.75	19.94
H−3	−1.90	76.28	3.76	19.97	−2.32	5.81	92.83	1.36	−2.62	4.30	93.80	1.90
H−4	−2.15	5.68	93.20	1.12	−2.52	0.03	99.95	0.02	−3.05	0.45	0.68	98.86

[a]All energies have been converted to the NHE scale assuming that the NHE potential is −4.5 V vs vacuum level.[29] [b]H = HOMO; L = LUMO.

29500, and 22500 cm^{-1}. The absorption spectra simulated from the results of TD-DFT calculations reproduce well the character of the experimental spectra (Figure 5) and thus can be used to assign the experimentally observed transitions (Tables 4−6).

In each case, the intense absorption band at higher energy (around 35000 cm^{-1}) is attributed to spin-allowed intraligand $\pi-\pi^*$ transitions, with some contribution from ligand-to-ligand charge transfer (LLCT) transitions. The lowest-energy band around 22500 cm^{-1} is due to the metal-to-ligand charge transfer (MLCT) transitions, as commonly seen in the optical spectra of Ru polypyridyl complexes. In contrast to those of **2** and **3**, the MLCT band of **1** reveals a low-energy tail that extends below 20000 cm^{-1}. This feature is attributed to the intraligand charge transfer (ILCT) excitation from the TTF-centered HOMO to the phenanthroline-centered LUMO+1.

The intermediate-energy band in the optical spectrum of **2** differs significantly from those found in the spectra of **1** and **3**. In the latter two complexes, this band appears as a broad shoulder at ~29500 cm^{-1} on the tail of the intense higher-energy band. In the spectrum of **2**, this band is red-shifted to 26000 cm^{-1}. Given the chemical similarity between complexes **2** and **3**, one would have to attribute this bathochromic shift to the substantial change in the bonding character when going from the C═S bond in **2** to the C═O and C═C bonds in **3** and **1**, respectively. Indeed, an examination of excitations that compose the intermediate-energy band confirms this assumption. In the case of **1**, this band involves a mix of transitions of MLCT (Ru → phen, Ru → bpy), LLCT (TTF → bpy), and ILCT (TTF → phen) character, which correspond to excitations from the Ru-based HOMO−1, HOMO−2, or HOMO−3, or from the TTF-based HOMO to the polypyridyl-centered π^* orbitals (Table 4). In both **2** and **3**, this band includes MLCT (Ru → bpy) and ILCT (TTC → phen or DTC → phen, respectively) transitions (Tables 5 and 6), but in **2**, the band is dominated by a strong HOMO−3 to LUMO+3 excitation that corresponds to the $\pi-\pi^*$ transition of the TTC fragment. Thus, the red shift of the intermediate-energy band in **2** relative to the corresponding bands in **1** and **3** stems from the stabilization of one of the unoccupied π^* orbitals (LUMO+3 in **2**) upon introduction of the additional S atom in **L2**.

Photophysical Properties. Complexes **1**−**3** exhibit luminescence in a CH_3CN solution at room temperature (Supporting Information, Figure S4) when excited at 450 nm (22220 cm^{-1}). The emissions appear as broad and structureless bands centered at ca. 600 nm (16670 cm^{-1}), which is characteristic of ^{3}MLCT

dx.doi.org/10.1021/ic4006949 | Inorg. Chem. 2013, 52, 8040−8052

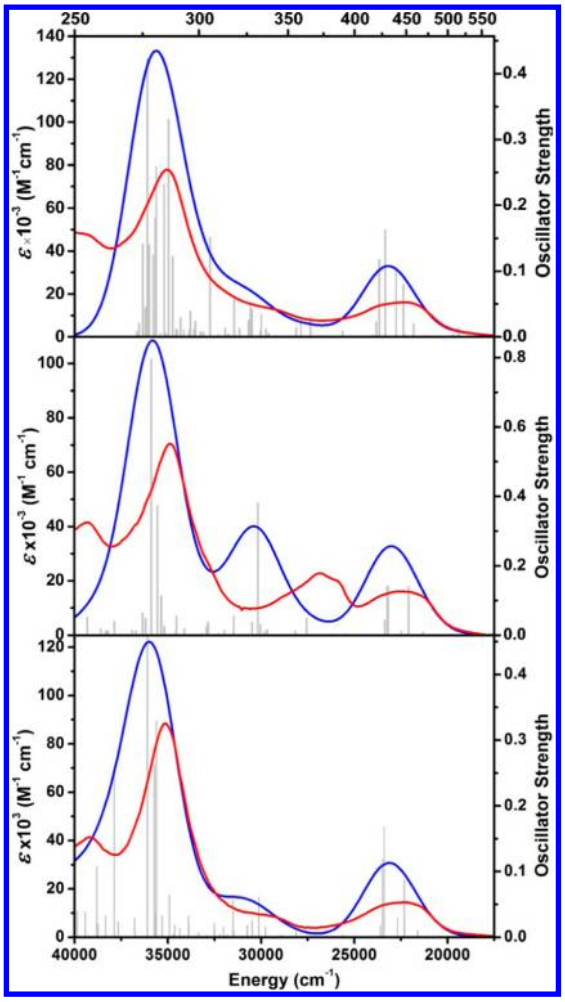

Figure 5. Experimental (red line) and simulated (blue line) optical absorption spectra of **1**−**3** (top to bottom, respectively). The gray bars indicate the energy and oscillator strength of each electronic excitation.

emission in Ru polypyridine complexes.[30] In comparison to reference complexes $[Ru(bpy)_3](PF_6)_2$ and $[Ru(bpy)_2(phen)](PF_6)_2$, the emission maximum ($\lambda_{em}$) of **1**−**3** is red-shifted by ∼400 cm^{-1}. The emission of complex **1** is shifted to a lower energy relative to those of **2** and **3**, which agrees with the smaller HOMO−LUMO gap in the former. Compiled in Table 7 are the photophysical properties of complexes **1**−**3** and the reference compounds. The emission lifetime (τ_{obs}) and quantum efficiency (Φ_F) of **1** in deoxygenated CH_3CN at room temperature are 1.77(4) μs and 1.2%, respectively. For **2** and **3**, these parameters are 1.47 μs and 6.6% and 2.08(4) μs and 9.7%, respectively.

The radiative lifetimes (τ_r) of **2** and **3** are 22 and 21 μs, respectively, as calculated from the respective quantum efficiencies and observed lifetimes. These τ_r values are of the order usually observed for the spin-forbidden transition from the ^{3}MLCT state of Ru(II) polypyridyl complexes.[31] For **1**, the observed lifetime (τ_{obs}) is comparable to those of **2** and **3**, but the overall luminescence quantum yield is significantly quenched. On the basis of the absorption spectra of the three compounds, the radiative lifetime of the ^{3}MLCT state of **1** is expected to be similar to those calculated for **2** and **3**. Therefore, the reduced luminescence quantum efficiency of **1** must be due to a nonradiative decay to a state at lower or similar energy competing with the intersystem crossing from the initially excited ^{1}MLCT states to the ^{3}MLCT state.[27]

The luminescence quenching observed for complex **1** may be associated with the different nature of frontier orbitals in **1** as compared to those of **2** and **3** (see Figure 4 and the related discussion above). In the latter complexes, the lowest-energy excitations, $Ru^{2+} \rightarrow$ bpy and $Ru^{2+} \rightarrow$ phen, correspond to the population of nearly degenerate ^{1}MLCT states, bpy/bpy$^{\bullet-}$-Ru^{3+}-phen and $(bpy)_2$-Ru^{3+}-phen$^{\bullet-}$, respectively, that are known to relax via intersystem crossing (ISC) and interligand electron hopping to the lowest-energy emissive ^{3}MLCT state.[32,33] In the case of **1**, however, the ISC can be quenched by electron transfer from the TTF donor moiety to the Ru^{3+} center, thus resulting in the decreased luminescence quantum yield. The mechanism of

Table 4. Assignments of Optical Absorption Bands of 1 Based on TD-DFT Calculations

	λ (nm)			
E (cm^{-1})	observed ($\varepsilon \times 10^{-4}$, M^{-1} cm^{-1})	calcd (osc. strength)	excitation	assignment
19194	521 (0.24)	515 (0.014)	H → L+1 (66%)	TTF → phen
22321	448 (1.62)	447 (0.080)	H−2 → L (41%)	Ru → phen
		439 (0.102)	H−3 → L+1 (38%)	Ru → phen
			H−2 → L+2 (37%)	Ru → bpy
		428 (0.163)	H−3 → L+2 (52%)	Ru → bpy
			H−2 → L+3 (38%)	Ru → bpy
		422 (0.118)	H−3 → L+1 (55%)	Ru → phen
			H−3 → L+3 (38%)	Ru → bpy
29155	343 (1.25)	333 (0.035)	H → L+8 (55%)	TTF → bpy
		328 (0.042)	H−1 → L+8 (63%)	Ru → bpy
		327 (0.054)	H → L+9 (57%)	TTF → phen
		318 (0.062)	H−2 → L+6 (47%)	Ru → bpy
		305 (0.152)	H−3 → L+7 (34%)	Ru → bpy
			H−2 → L+9 (33%)	Ru → phen
35088	285 (7.78)	286 (0.331)	H−9 → L+1 (33%)	phen → phen
		284 (0.233)	H−4 → L+4 (54%)	TTF → bpy
		281 (0.259)	H−7 → L+3 (41%)	bpy → bpy

dx.doi.org/10.1021/ic4006949 | Inorg. Chem. 2013, 52, 8040−8052

Table 5. Assignments of Optical Absorption Bands of 2 Based on TD-DFT Calculations

	λ (nm)			
E (cm^{-1})	observed ($\varepsilon \times 10^{-4}$, M^{-1} cm^{-1})	calcd (osc. strength)	excitation	assignment
22573	443 (1.74)	449 (0.140)	H−1 → L (50%)	Ru → phen
		428 (0.142)	H−1 → L+1 (48%)	Ru → phen
			H−2 → L+2 (42%)	Ru → bpy
		427 (0.140)	H−2 → L+1 (51%)	Ru → phen
			H−2 → L+4 (37%)	Ru → bpy
26882	372 (2.41)	361 (0.049)	H−3 → L+1 (66%)	TTC → phen
25974	385 (2.13) sh	332 (0.031)	H → L+6 (60%)	Ru → bpy
		330 (0.382)	H−3 → L+3 (58%)	TTC → TTC
		327 (0.038)	H → L+8 (61%)	Ru → bpy
		317 (0.057)	H−1 → L+6 (45%)	Ru → bpy
34965	286 (8.09)	289 (0.056)	H−5 → L+2 (52%)	bpy → bpy
		282 (0.114)	H−7 → L (57%)	phen → phen
		278 (0.798)	H−5 → L+4 (41%)	bpy → bpy
		276 (0.050)	H−3 → L+5 (59%)	TTC → bpy
		275 (0.065)	H−7 → L+3 (47%)	phen → TTC
		254 (0.053)	H−2 → L+11 (62%)	Ru → phen

Table 6. Assignments of Optical Absorption Bands of 3 Based on TD-DFT Calculations

	λ (nm)			
E, cm^{-1}	observed ($\varepsilon \times 10^{-4}$, M^{-1} cm^{-1})	calcd (osc. strength)	excitation	assignment
22573	443 (1.67)	448 (0.088)	H−1 → L (42%)	Ru → phen
		427 (0.169)	H−2 → L+2 (52%)	Ru → bpy
			H−1 → L+1 (32%)	Ru → phen
		426 (0.119)	H−2 → L+1 (53%)	Ru → phen
			H−2 → L+3 (38%)	Ru → bpy
29412	340 (0.97)	332 (0.062)	H−3 → L+1 (63%)	DTC → phen
		317 (0.057)	H−1 → L+6 (45%)	Ru → bpy
35211	284 (10.26)	286 (0.065)	H−6 → L+1 (52%)	DTC → phen
		281 (0.330)	H−5 → L+3 (50%)	bpy → bpy
		280 (0.263)	H−6 → L (37%)	DTC → phen
		277 (0.825)	H−6 → L (39%)	DTC → phen
		264 (0.258)	H−3 → L+4 (60%)	DTC → bpy
		258 (0.109)	H−3 → L+5 (63%)	DTC → DTC

Table 7. Photophysical Properties[a] of Complexes 1−3 and Reference Compounds $[Ru(bpy)_3](PF_6)_2$ and $[Ru(bpy)_2(phen)](PF_6)_2$[26]

complex	E_{MLCT} (cm^{-1})/λ_{MLCT} (nm) ($\varepsilon \times 10^{-4}$ (M^{-1} cm^{-1}))	E_{em} (cm^{-1})/λ_{em} (nm)	ν_{ST} (cm^{-1})	Φ_F (%)	τ_{obs} (μs)	τ_r (μs)	τ_{nr} (μs)	k_r (s^{-1})	k_{nr} (s^{-1})
1	22321/448 (1.62)	15723/636	6598	1.2	1.77(4)				
2	22573/443 (1.74)	15823/632	6750	6.6	1.47(4)	22	1.58	4.5×10^4	6.4×10^5
3	22573/443 (1.67)	15898/629	6675	9.7	2.08(4)	21	2.31	4.7×10^4	4.3×10^5
$[Ru(bpy)_3](PF_6)_2$	22172/451 (1.32)	16260/615	5912	6.2	0.86	14	0.92	7.2×10^4	1.1×10^6
$[Ru(bpy)_2(phen)](PF_6)_2$	22271/449 (1.57)	16340/612	5931	6.0	0.80	13	0.85	7.5×10^4	1.2×10^6

[a] E_{MLCT}/λ_{MLCT} = energy/wavelength of maximum MLCT absorption; E_{em}/λ_{em} = energy/wavelength of maximum emission; ν_{ST} = Stokes shift; Φ_F = luminescence relative quantum yield under 450 nm excitation, using $[Ru(bpy)_3]^{2+}$ in CH_3CN as a standard with $\Phi_f = 0.062$; τ_{obs} = measured luminescence lifetime; τ_r = calculated radiative lifetime ($\Phi_F = \tau_{obs}/\tau_r$); τ_{nr} = calculated nonradiative lifetime ($1/\tau_r + 1/\tau_{nr} = 1/\tau_{obs}$); k_r = radiative rate constant ($k_r = \Phi_F/\tau_{obs}$); k_{nr} = nonradiative rate constant ($k_r + k_{nr} = 1/\tau_{obs}$).

such quenching requires special attention. The initial excitation from the ground state of **1** also creates two ^{1}MLCT states, $(bpy)_2$-Ru^{2+}-$phen^{\bullet-}$-TTF^+ ($^1MLCT_1$) and bpy/$bpy^{\bullet-}$-Ru^{3+}-phen-TTF ($^1MLCT_2$), which have quite different natures because of the presence of the TTF moiety in the vicinity of the excited electron in $^1MLCT_1$ (Scheme 2). In the $^1MCLT_2$ state, the electron can be transferred from TTF to Ru^{3+} to produce, in a cascade, first a lower-energy, charge-separated

dx.doi.org/10.1021/ic4006949 | Inorg. Chem. 2013, 52, 8040−8052

Scheme 2. Energy Level Scheme for the Charge Transfer States Prevalent in 1 upon Excitation[a]

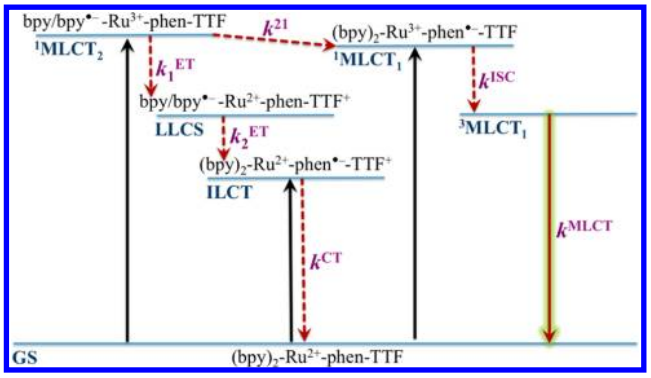

[a]GS = ground state; MLCT = metal-to-ligand charge transfer excited states; LLCS = ligand-to-ligand charge-separated excited state; ILCT = intraligand charge transfer excited state. The most probable radiative and nonradiative relaxation pathways are depicted as solid and dashed red arrows, respectively.

LLCT state, bpy/bpy$^{\bullet-}$-Ru^{2+}-phen-TTF^{+}, and finally a nonemissive ILCT state, (bpy)$_2$-Ru^{2+}-phen$^{\bullet-}$-TTF^{+}. For the (bpy)$_2$-Ru^{3+}-phen$^{\bullet-}$-TTF (^{1}MCLT$_1$) state, the TTF → Ru^{3+} electron transfer is expected to be slower because of the localization of the excited-state electron on the phen moiety. This blockage of the electron transfer results in more efficient ISC to the corresponding ^{3}MLCT$_1$ state that undergoes the radiative decay with the characteristic lifetime of 1.77 μs.

In principle, the TTF → Ru^{3+} electron transfer can also occur in the corresponding longer-lived ^{3}MLCT$_2$ state, and it would be of interest to investigate the possible competition of this process with the radiative decay by combining advanced transient spectroscopy and theoretical calculations. However, on the basis of the spectroscopic and the electrochemical data, the driving force for electron transfer in the ^{3}MLCT$_2$ state would be significantly smaller than in the ^{1}MLCT$_2$ state. Therefore, this process would be slower and would have to compete with the electron localization in the lowest-energy ^{3}MLCT state, namely the ^{3}MLCT$_1$ state, via interligand electron hopping on the picosecond time scale.[33] This puts the electron transfer rate into direct competition with the ^{1}MLCT to ^{3}MLCT ISC. Thus, we believe that the luminescence quenching in complex **1** stems primarily from the inability of the ^{1}MLCT$_2$ state to undergo ISC to the corresponding ^{3}MLCT$_2$ state.

In an effort to better understand the nature of the luminescence (and thus the quenching mechanism) of **1**, time-resolved transient absorption spectra were collected in a deaerated CH_3CN solution at room temperature.[34] A 488 nm (20492 cm^{-1}) pulse into the tail of the mixed Ru → phen/Ru → bpy ^{1}MLCT band was used for excitation, and the bleach of this band was monitored at 458 nm (21834 cm^{-1}). There is no indication of an intermediate state in the transient signal, and the kinetic trace was fit to a single exponential (Figure 6) with a lifetime of 1.75(7) μs, which coincides with the luminescence lifetime of **1** (Table 7). Unfortunately, there is no indication of an intermediate charge-separated state that would be sufficiently long-lived on the scale of the detection limits of the instrument (>10 ns). If such a state exists, experiments on a faster time scale will be required to observe it.

We also probed a transient signal at 370 nm (27027 cm^{-1}) under 488 nm excitation. At this energy, the reference compound [Ru(bpy)$_3$](PF$_6$)$_2$ exhibits a significant transient absorption

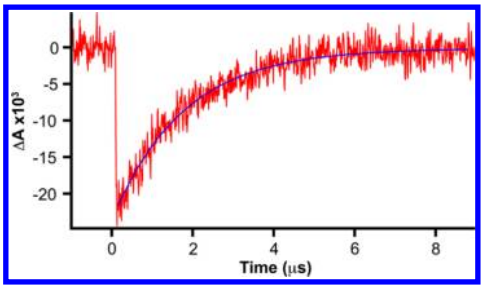

Figure 6. Kinetic profile of the difference absorbance spectrum of **1** in CH_3CN at room temperature. λ_{pump} = 488 nm; λ_{probe} = 458 nm. Experimental data, red; single exponential fit, blue.

signal.[35] In the case of **1**, however, we observed only a very weak signal at 370 nm, which decayed at a single-exponential rate but with a high degree of uncertainty: 1.6(8) μs (Supporting Information, Figure S5). This observation reinforces our assumption that the luminescence of **1** is of the ^{3}MLCT nature.

Photodegradation of the TTF-Containing Complex 1. The solid form of **1** can be stored in air for a prolonged period of time without any visible degradation, but when dark red crystals of **1** were left under O_2-saturated mother liquor (CH_3CN/Et_2O) for about a week, a complete transformation of this compound to a new orange crystalline solid was observed. The crystal structure determination revealed that the TTF fragment of **1** had undergone an oxidative cleavage of the central C═C bond, resulting in the complete transformation of **1** to **3**.

To investigate the cause of this unexpected transformation, ^{13}C NMR spectroscopy was utilized to monitor CD_3CN solutions of **1** as well as control CH_2Cl_2 solutions of **L1**, kept under ambient light and in the dark (Figure 7). The experiment

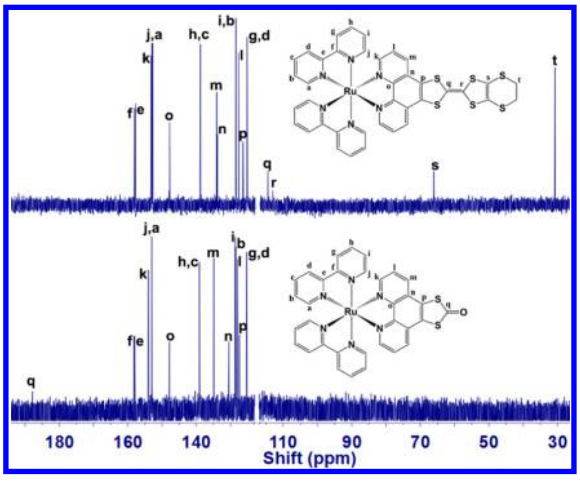

Figure 7. ^{13}C NMR spectra of **1** in $CDCl_3$ before (top) and after (bottom) being exposed to light and air for a period of 20 days.

monitored solutions kept in both air-saturated and air-free environments. An analysis of the ^{13}C NMR spectra showed that **1** remained intact in solutions kept in air-free or dark environments for 3 weeks but converted to **3** in solutions exposed to air and light. Furthermore, upon conversion, the portion of **L1** cleaved from the Ru(II) complex precipitated as a light orange solid. This solid was filtered prior to obtaining the final NMR spectrum, which explains the absence of peaks for the corresponding carbons (labeled **r**, **s**, and **t** in Figure 7). There is also a substantial change in the chemical shift of carbon **q** upon conversion, from 115 to 188 ppm, as expected for the formation of the carbonyl

dx.doi.org/10.1021/ic4006949 | Inorg. Chem. 2013, 52, 8040−8052

carbon upon transformation. The free ligand **L1** did not show decomposition in any of the solutions tested (i.e., its ^{13}C NMR spectra remained unchanged after 3 weeks). These results indicate the need for the presence of the photoactive Ru^{II} ion for the transformation of **L1** to **L3**.

Taking into account the difference in the photophysical properties of **1** and **3** (Table 7), we recorded absorption and emission spectra of a CH_3CN solution of **1** before and after irradiation for 4 h with a 458 nm pulsed laser (Figure 8). The

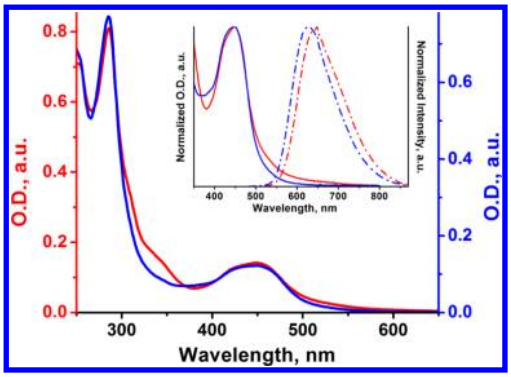

Figure 8. Absorption (solid lines) and emission (dashed lines) spectra of **1** in a CH_3CN solution before (red) and after (blue) pulsed-laser irradiation at 458 nm for a period of 4 h.

attenuation of both the low-energy tail of the MLCT band above 500 nm and the mixed ILCT/LLCT band (TTF → phen/bpy, Table 4) that appears as a shoulder at 340 nm, along with the hypsochromic shift of the emission maximum from 642 to 630 nm, is in accord with the conversion of **1** to **3**. A control experiment was also performed on a CH_3CN solution of **1** that was kept in a dark and O_2-free environment. The absorption and emission spectra of this solution remained essentially unchanged after the 4 h period without irradiation (Supporting Information, Figure S6), yet again confirming the necessity of irradiation for the oxidative cleavage of the C═C bond in the TTF unit of **1**.

Given the difference in the luminescence lifetimes of **1** and **3** (1.77(4) and 2.08(4) μs, respectively), we monitored the change in this parameter for a deaerated CH_3CN solution of **1** under continuous irradiation with the 458 nm pulsed laser for 4 h (Figure 9). During this period, the sample was kept in a capped cuvette. The initial measurement was performed immediately after degassing the solution and prior to turning on the laser. It resulted in τ_{obs} = 1.74(5) μs, as expected for the deaerated

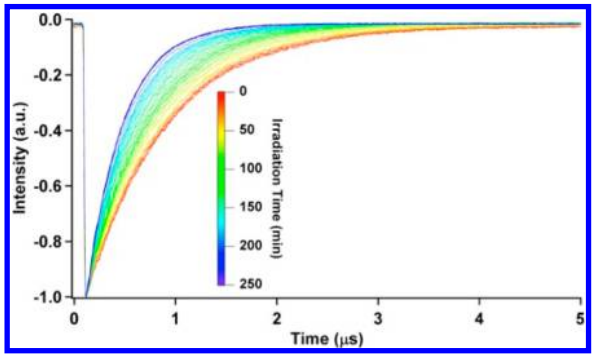

Figure 9. Monitoring the luminescence decay at 640 nm (λ_{exc} = 458 nm) of a 10 μM solution of **1** in CH_3CN at 298 K. Sample cuvette was exposed to pulsed irradiation for a period of 4 h.

solution of **1** (Table 7). The continuous irradiation led to a gradual decrease in the luminescence lifetime until it reached a constant value of 0.353(3) μs after 4 h of irradiation. The substantial decrease in the luminescence lifetime points toward the incidental seepage of atmospheric oxygen into the cuvette, which results in substantial luminescence quenching.[36] Thus, the luminescence decay of a freshly prepared and degassed CH_3CN solution of **1** was measured immediately after the solution was exposed to air under visible light, resulting in τ_{obs} = 0.279(4) μs. This value, however, is significantly shorter than the value of 0.353(3) μs obtained for the solution kept in a capped cuvette under irradiation for 4 h. Because the presence of oxygen and irradiation can also result in the photodegradation of **1** to **3**, the same measurement was performed on a degassed CH_3CN solution of **3** immediately after it was exposed to air. The measured τ_{obs} = 0.358(8) μs is substantially shorter than the 2.08(4) μs value obtained for a deaerated solution of **3** (Table 7). Nevertheless, it is in excellent agreement with the value of 0.353(3) μs observed after continuously irradiating the CH_3CN solution of **1** in a capped cuvette for 4 h. These results confirm our initial assumption about the slow photodegradation of **1** to **3** due to the seepage of air into the cuvette. They also indicate that the photodegradation process occurs quite fast once the solution is exposed to air under visible light.

CONCLUSIONS

A detailed study of Ru(II) complexes with redox-active TTF-annulated phenanthroline (edt-TTF-phen, **L1**) and its analogues that contain only half of the TTF unit (TTC-phen, **L2**, and DTC-phen, **L3**) reveals that $[Ru(bpy)_2(\mathbf{L1})](PF_6)_2$ (**1**) exhibits behavior distinctly different from that observed for $[Ru(bpy)_2(\mathbf{L2})](PF_6)_2$ (**2**) and $[Ru(bpy)_2(\mathbf{L3})](PF_6)_2$ (**3**). This difference stems from the presence of an additional redox-active MO in **1** which is centered on the TTF unit, serving as the HOMO, and which is located ~0.6 eV above the Ru-based d orbitals. Such a high-energy ligand-centered HOMO is absent in **2** and **3**. Consequently, **1** exhibits three reversible oxidations, of which the two occurring at lower potentials are TTF-based. A low-energy tail of the MLCT absorption band, observed only for **1**, is assigned to the ILCT within the **L1** ligand, according to TD-DFT calculations. Upon irradiation into the characteristic low-energy MLCT band, complexes **1**−**3** exhibit emission with luminescence lifetimes of ~1−2 μs. The monoexponential rate of luminescence decay indicates that the MLCT state is the only one contributing to the observed emission. In contrast to **2** and **3**, complex **1** also experiences intramolecular reductive excited-state electron transfer from the TTF moiety to the Ru center. This process is evident from the substantially lower luminescence quantum yield of **1** (Φ_F = 0.012) when compared to those of **2** and **3** and the reference compounds $[Ru(bpy)_3](PF_6)_2$ and $[Ru(bpy)_2(phen)](PF_6)_2$ (Φ_F = 0.060−0.095). This finding is in agreement with the well-established electron-donating properties of TTF. Contrary to expectations from the previous reports on related Ru(II) complexes with TTF-containing ligands, the presence of the low-energy ILCT state (TTF → phen) is not accompanied by a long-lived charge-separated state (>10 ns) that is detectable as a transient species when probing the excited-state absorbance profile. Solutions of **1** exposed to air and visible light exhibit photodegradation that leads to the cleavage of the central C═C bond of the TTF unit and quantitative generation of **3**.

The interesting photophysical behavior of complex **1** and the related previously reported complex, $Ru(bpy)_2(TTF\text{-}dppz)](PF_6)_2$,[27] call for further studies of heteroleptic Ru(II) complexes

dx.doi.org/10.1021/ic4006949 | Inorg. Chem. 2013, 52, 8040−8052

with redox-active ligands. In particular, we are currently investigating the nature of excited states in these and related complexes by ultrafast spectroscopy and more thorough theoretical calculations. The results of these studies will be reported in due course.

■ ASSOCIATED CONTENT

Ⓢ Supporting Information

^{1}H and 2D COSY NMR spectra of **1**−**3**, molecular structure of $[Ru(bpy)_2(\mathbf{L1})]^{2+}$, crystal packing of **L1**, emission spectra of complexes **1**−**3**, kinetic profile of the difference absorbance spectrum of **1**, and absorption and emission spectra of a control CH_3CN solution of **1**. This material is available free of charge via the Internet at http://pubs.acs.org.

■ AUTHOR INFORMATION

Corresponding Author

*E-mail: andreas.hauser@unige.ch (A.H.), shatruk@chem.fsu.edu (M.S.).

Present Addresses

[§]K.K.: Department of Chemistry, University of California at Davis, Davis, CA 95616.

[∥]J.M.H.: Department of Chemistry, Princeton University, Princeton, NJ 08544.

Notes

The authors declare no competing financial interest.

■ ACKNOWLEDGMENTS

This research was partially supported by the National Science Foundation (award CHE-0911109 to M.S.).

■ REFERENCES

(1) (a) Coronado, E.; Galán-Mascarós, J. R. *J. Mater. Chem.* **2005**, *15*, 66−74. (b) Ouahab, L. N.; Enoki, T. *Eur. J. Inorg. Chem.* **2004**, 933−941. (c) Coronado, E.; Galán-Mascarós, J. R.; Gómez-García, C. J.; Laukhin, V. *Nature* **2000**, *408*, 447−449. (d) Branzea, D. G.; Fihey, A.; Cauchy, T.; El-Ghayoury, A.; Avarvari, N. *Inorg. Chem.* **2012**, *51*, 8545−8556. (e) Lee, B. I.; Lee, E. S.; Byeon, S. H. *Adv. Funct. Mater.* **2012**, *22*, 3562−3569. (f) Li, W.; Yang, J. P.; Wu, Z. X.; Wang, J. X.; Li, B.; Feng, S. S.; Deng, Y. H.; Zhang, F.; Zhao, D. Y. *J. Am. Chem. Soc.* **2012**, *134*, 11864−11867. (g) Murata, T.; Nakasuji, K.; Morita, Y. *Eur. J. Org. Chem.* **2012**, 4123−4129. (h) Pacchioni, G. *Chem.—Eur. J.* **2012**, *18*, 10144−10158.

(2) (a) Perepichka, D. F.; Bryce, M. R.; Pearson, C.; Petty, M. C.; McInnes, E. J. L.; Zhao, J. P. *Angew. Chem., Int. Ed.* **2003**, *42*, 4636−4639. (b) Rabaça, S.; Almeida, M. *Coord. Chem. Rev.* **2010**, *254*, 1493−1508. (c) Riobé, F.; Avarvari, N. *Coord. Chem. Rev.* **2010**, *254*, 1523−1533. (d) Lorcy, D.; Bellec, N.; Fourmigué, M.; Avarvari, N. *Coord. Chem. Rev.* **2009**, *253*, 1398−1438. (e) Kobayashi, H.; Cui, H. B.; Kobayashi, A. *Chem. Rev.* **2004**, *104*, 5265−5288. (f) Bendikov, M.; Wudl, F.; Perepichka, D. F. *Chem. Rev.* **2004**, *104*, 4891−4945.

(3) Rivera, N. M.; Engler, E. M.; Schumaker, R. R. *J. Chem. Soc., Chem. Commun.* **1979**, 184−185.

(4) Nagawa, T.; Zama, Y.; Okamoto, Y. *Bull. Chem. Soc. Jpn.* **1984**, *57*, 2035−2036.

(5) Iwahori, F.; Golhen, S.; Ouahab, L.; Carlier, R.; Sutter, J. P. *Inorg. Chem.* **2001**, *40*, 6541−6542.

(6) (a) Fourmigué, M.; Batail, P. *Bull. Soc. Chim. Fr.* **1992**, *129*, 29−36. (b) Ebihara, M.; Nomura, M.; Sakai, S.; Kawamura, T. *Inorg. Chim. Acta* **2007**, *360*, 2345−2352.

(7) (a) Jørgensen, T.; Becher, J.; Chambron, J. C.; Sauvage, J. P. *Tetrahedron Lett.* **1994**, *35*, 4339−4342. (b) Bang, K. S.; Nielsen, M. B.; Zubarev, R.; Becher, J. *Chem. Commun.* **2000**, 215−216.

(8) Keniley, L. K., Jr.; Ray, L.; Kovnir, K.; Dellinger, L. A.; Hoyt, J. M.; Shatruk, M. *Inorg. Chem.* **2010**, *49*, 1307−1309.

(9) Fulmer, G. R.; Miller, A. J. M.; Sherden, N. H.; Gottlieb, H. E.; Nudelman, A.; Stoltz, B. M.; Bercaw, J. E.; Goldberg, K. I. *Organometallics* **2010**, *29*, 2176−2179.

(10) Varma, K. S.; Bury, A.; Harris, N. J.; Underhill, A. E. *Synthesis* **1987**, 837−838.

(11) Qin, J.; Hu, L.; Li, G.-N.; Wang, X.-S.; Xu, Y.; Zuo, J.-L.; You, X.-Z. *Organometallics* **2011**, *30*, 2173−2179.

(12) (a) *SMART*, revision 5.62; Bruker ASX Inc.: Madison, WI, 2007. (b) *SAINT*, revision 6.02; Bruker ASX Inc.: Madison, WI, 2007.

(13) Sheldrick, G. M. *SADABS*, revision 2.03; University of Gottingen: Gottingen, Germany, 1996.

(14) Sheldrick, G. M. *Acta Crystallogr., Sect. A: Found. Crystallogr.* **2008**, *A64*, 112−122.

(15) Frisch, M. J.; Trucks, G. W.; Schlegel, H. B.; Scuseria, G. E.; Robb, M. A.; Cheeseman, J. R.; Montgomery, J. A., Jr.; Vreven, T.; Kudin, K. N.; Burant, J. C.; Millam, J. M.; Iyengar, S. S.; Tomasi, J.; Barone, V.; Mennucci, B.; Cossi, M.; Scalmani, G.; Rega, N.; Petersson, G. A.; Nakatsuji, H.; Hada, M.; Ehara, M.; Toyota, K.; Fukuda, R.; Hasegawa, J.; Ishida, M.; Nakajima, T.; Honda, Y.; Kitao, O.; Nakai, H.; Klene, M.; Li, X.; Knox, J. E.; Hratchian, H. P.; Cross, J. B.; Bakken, V.; Adamo, C.; Jaramillo, J.; Gomperts, R.; Stratmann, R. E.; Yazyev, O.; Austin, A. J.; Cammi, R.; Pomelli, C.; Ochterski, J. W.; Ayala, P. Y.; Morokuma, K.; Voth, G. A.; Salvador, P.; Dannenberg, J. J.; Zakrzewski, V. G.; Dapprich, S.; Daniels, A. D.; Strain, M. C.; Farkas, O.; Malick, D. K.; Rabuck, A. D.; Raghavachari, K.; Foresman, J. B.; Ortiz, J. V.; Cui, Q.; Baboul, A. G.; Clifford, S.; Cioslowski, J.; Stefanov, B. B.; Liu, G.; Liashenko, A.; Piskorz, P.; Komaromi, I.; Martin, R. L.; Fox, D. J.; Keith, T.; Al-Laham, M. A.; Peng, C. Y.; Nanayakkara, A.; Challacombe, M.; Gill, P. M. W.; Johnson, B.; Chen, W.; Wong, M. W.; Gonzalez, C.; Pople, J. A. *Gaussian 03*, revision B.03; Gaussian, Inc.: Wallingford, CT, 2004.

(16) (a) Becke, A. D. *Phys. Rev. A* **1988**, *38*, 3098−3100. (b) Lee, C.; Yang, W.; Parr, R. G. *Phys. Rev. B* **1988**, *37*, 785−789.

(17) (a) Dunning, T. H., Jr.; Hay, P. J. *Mod. Theor. Chem.* **1977**, *3*, 1−27. (b) Hay, P. J.; Wadt, W. R. *J. Chem. Phys.* **1985**, *82*, 270−283. (c) Hay, P. J.; Wadt, W. R. *J. Chem. Phys.* **1985**, *82*, 299−310. (d) Wadt, W. R.; Hay, P. J. *J. Chem. Phys.* **1985**, *82*, 284−298.

(18) (a) Gorelsky, S. I. *SWizard*, revision 4.6; University of Ottawa: Ottawa, Canada, 2010. (b) Gorelsky, S. I.; Lever, A. B. P. *J. Organomet. Chem.* **2001**, *635*, 187−196.

(19) Gorelsky, S. I. *AOMix: Program for Molecular Orbital Analysis*, version 6.5; University of Ottawa: Ottawa, Canada, 2011.

(20) Rabaça, S.; Duarte, M. C.; Santos, I. C.; Pereira, L. C. J.; Fourmigué, M.; Henriques, R. T.; Almeida, M. *Polyhedron* **2008**, *27*, 1999−2006.

(21) Chesneau, B.; Passelande, A.; Hudhomme, P. *Org. Lett.* **2009**, *11*, 649−652.

(22) Jeppesen, J. O.; Takimiya, K.; Jensen, F.; Brimert, T.; Nielsen, K.; Thorup, N.; Becher, J. *J. Org. Chem.* **2000**, *65*, 5794−5805.

(23) Our repeated attempts to prepare a symmetric bis-phenanthroline ligand by self-coupling of **L2** or **L3** or their cross-coupling to each other have failed to produce the desired product. The same failure was reported by Hudhomme et al.[21] It remains unclear whether the lack of success in these reactions stems from the extremely low solubility of the symmetric (and likely planar) phen-TTF-phen molecule, or if the reaction simply does not proceed.

(24) Ye, B.-H.; Ji, L.-N.; Xue, F.; Mak, T. C. W. *Transition Met. Chem. (Dordrecht, Neth.)* **1999**, *24*, 8−12.

(25) Bryce, M. R.; Marshallsay, G. J.; Moore, A. J. *J. Org. Chem.* **1992**, *57*, 4859−4862.

(26) Bomben, P. G.; Robson, K. C. D.; Sedach, P. A.; Berlinguette, C. P. *Inorg. Chem.* **2009**, *48*, 9631−9643.

(27) Goze, C.; Leiggener, C.; Liu, S.-X.; Sanguinet, L.; Levillain, E.; Hauser, A.; Decurtins, S. *ChemPhysChem.* **2007**, *8*, 1504−1512.

(28) (a) Wilson, G. J.; Will, G. D. *Inorg. Chim. Acta* **2010**, *363*, 1627−1638. (b) Gorelsky, S. I.; Lever, A. B. P. *J. Organomet. Chem.* **2001**, *635*, 187−196. (c) Lever, A. B. P.; Gorelsky, S. I. *Struct. Bonding (Berlin, Ger.)* **2004**, *107*, 77−114. (d) Allard, M. M.; Odongo, O. S.; Lee, M. M.; Chen, Y.-J.; Endicott, J. F.; Schlegel, H. B. *Inorg. Chem.* **2010**, *49*, 6840−6852. (e) Guillemoles, J.-F.; Barone, V.; Joubert, L.; Adamo, C. *J. Phys. Chem. A*

2002, *106*, 11354−11360. (f) Very, T.; Despax, S.; Hébraud, P.; Monari, A.; Assfeld, X. *Phys. Chem. Chem. Phys.* **2012**, *14*, 12496−12504.
(29) Grätzel, M. *Nature* **2001**, *414*, 338−344.
(30) (a) Campagna, S.; Puntoriero, F.; Nastasi, F.; Bergamini, G.; Balzani, V. *Top. Curr. Chem.* **2007**, *280*, 117−214. (b) Juris, A.; Balzani, V.; Barigelletti, F.; Campagna, S.; Belser, P.; Vonzelewsky, A. *Coord. Chem. Rev.* **1988**, *84*, 85−277. (c) Kalyanasundaram, K. *Coord. Chem. Rev.* **1982**, *46*, 159−244.
(31) (a) Bialkowski, S. E. Photothermal Spectroscopy Methods for Chemical Analysis. In *Chemical Analysis: A Series of Monographs on Analytical Chemistry and Its Applications*; Winefordner, J. D., Ed.; John Wiley & Sons: New York, 1996; Vol. *134*. (b) Bhasikuttan, A. C.; Suzuki, M.; Nakashima, S.; Okada, T. *J. Am. Chem. Soc.* **2002**, *124*, 8398−8405. (c) Strouse, G. F.; Schoonover, J. R.; Duesing, R.; Boyde, S.; Jones, W. E.; Meyer, T. J. *Inorg. Chem.* **1995**, *34*, 473−487. (d) Baba, A. I.; Shaw, J. R.; Simon, J. A.; Thummel, R. P.; Schmehl, R. H. *Coord. Chem. Rev.* **1998**, *171*, 43−59.
(32) Lytle, F. E.; Hercules, D. M. *J. Am. Chem. Soc.* **1969**, *91*, 253−257.
(33) Wallin, S.; Davidsson, J.; Modin, J.; Hammarstrom, L. *J. Phys. Chem. A* **2005**, *109*, 4697−4704.
(34) We collected kinetic traces at a specific wavelength, as opposed to monitoring the entire transient absorption spectrum, to minimize the influence of the probe on the photodegradation process occurring in **1**.
(35) Hauser, A.; Krausz, E. *Chem. Phys. Lett.* **1987**, *138*, 355−360.
(36) Mulazzani, Q. G.; Sun, H.; Hoffman, M. Z.; Ford, W. E.; Rodgers, M. A. J. *J. Phys. Chem.* **1994**, *98*, 1145−1150.